Synthesis and Characterization of CdS Nanostructures via CPM and PLAL

A.M. Darwish [a], W. H. Eisa [a], A. A. Shabaka [a], M. H. Talaat [b]

[a] Spectroscopy Department, Physics Division, National Research Center, Dokki, Cairo, Egypt
[b] Physics Department, Faculty of Science, Ain Shams University, Egypt

There are number of methods were developed to synthesize cadmium sulfide (CdS) materials in nanoscale such as chemical precipitation method (CPM) and pulsed laser ablation in a liquid solution (PLAL). In the CPM, with increasing the amount of ethylenediamine (en) acting as a surfactant from 25% to 100% the obtained CdS nanorods decrease in their axis and tends to take spherical shape at 100% of en. The results obtained from CPM were used for comparison with PLAL. In PLAL, with increasing the laser intensity of the used nanosecond laser the particles size of produced CdS is reduced and exhibits narrow particle size distribution.

Index Terms— Cadmium sulfide (CdS), Nanomaterials, Chemical precipitation method (CPM), Pulsed laser ablation in liquid environment (PLAL), nanosecond laser

1. Introduction

In the last few decades, researches on nanostructures have increased enormously and have been extremely attractive and interest to several fields of research because of their unique size-dependent optical, electronic properties, magnetic and chemical properties which are different from their bulk materials [1-4]. Important scientific and technological advances based on understanding and control of properties and processes at the scale of atoms and molecules, the nanometer scale, are taking place in laboratories around the world. The ability to control materials at the nanoscale is already leading to novel materials and improved performance and other characteristics in existing products. Over the longer term, nanotechnology promises even more revolutionary advances with potential impacts on nearly every industrial sector, including energy, health care, defense, transportation, and electronics.

Therefore nanostructures are predicted to be, or are already, successfully employed in a wide range of applications. Special the nanostructures made out of II–VI are important nanomaterials for optoelectronic, biosensing and imaging, magnetic and optical memory, nanoelectronics, hard coatings, chemical-mechanical polishing applications [2, 5-8]. In particular, when the size of the nanocrystallites is close to or smaller than the exciton Bohr radius within the corresponding bulk material, they are termed as quantum dots and exhibit very special physical and chemical properties [9].

Many attempts have been made by the researchers in the world to discover and develop the new synthesis methods and characterization techniques to control shape and size of nanostructures due to the heavily shape/size-dependent functional properties. nanostructures have been prepared by a wide variety of techniques such as pulsed laser deposition [10], flame metal combustion [11], chemical reduction [12], photo-reduction [13], electrochemical reduction [14], solvothermal [15], electrolysis [16], green method [17], Microwave-induced [18], sono-electrochemical [19], aerosol flow reactor [20], photochemical reduction [21], chemical fluid deposition [22], spray pyrolysis [23, 24], and spark discharge [25]. The usual techniques for synthesizing metallic nanostructures are chemical reactions. Recently, the new methods were developed to synthesize materials in nanoscale like pulsed laser ablation of metal target in a liquid solution (PLAL)[26].

Chemical Precipitation method (CPM) is the most common technology used to remove dissolved (ionic) metals from solutions. The ionic metals are converted to an insoluble form (particle) by the chemical reaction between the soluble metal compounds and the precipitating reagent. The particles formed by this reaction are removed from solution by settling and/or filtration. The unit operations typically required in this technology includes neutralization, precipitation, coagulation/flocculation, solids/liquid separation and dewatering.The effectiveness of CPM is dependent on several factors, including the type and concentration of ionic metals present in solution, the precipitant used, the reaction conditions and the presence of other constituents that may inhibit the precipitation reaction.

Pulsed laser ablation (PLA), Pulsed laser irradiation of a target (mostly solid), is the process by which macroscopic amounts of material are ejected from the surface of a solid irradiated by the interaction of relatively short (10^{-15}-10^{-9}s), intense (10^{9}-10^{14}Wcm^{-2}), laser pulse bursts of coherent and monochromatic light with surfaces, offers a unique way to perturb materials away from equilibrium [27].

In this work, our synthetic strategy of binary compound (CdS) by CPM is based upon the controlled, aqueous precipitation of cations (e.g. Cd^{2+}) with anions (e.g. S^{2-}) in the presence of a stabilizer (en). The surfactants adsorb to the growing crystal depending upon the precursor concentrations which can moderate the growth rate of crystal faces. Then we make a comparative study between these results and the nanofabrications results from PLAL method.

2. Materials and Experimental

2.1. Materials

Cadmium chloride hemipetahydrate ($CdCl_2.xH_2O$) of M.W. 228.35, 95%, Ltd., Sodium sulfide (Na_2S) of M.W. 78.03, Sulfur (S) of A.W.32.97, Ethylenediamine LR (1,2-diaminoethane), en, M.W 60.10, All of these chemicals from S. d. Fine-Chem were analytical grade and used without further purification.

3. Experimental

In CPM, 0.069g of Cadmium chloride hemipetahydrate ($CdCl_2.xH_2O$) was dissolved in 150mL of distilled water, which contains an appropriate amount of ethylenediamine (en) in a flask. After stirring the solution for about 15 min, 0.216g of Sodium sulfide (Na_2S) was added drop by drop in 30 minutes. A yellow color of the solution developed gradually when the reaction proceeded under constant stirring at 80°C. The stirring was continued further for 24 hours in order to facilitate complete nanoparticle precipitation. After the reaction was completed, the resulting solution was centrifuged and washed with distilled water and ethanol, respectively to get rid of unreacted species and byproduct. The sample was dried at 100 °C for 6 h. Then the free standing powder was collected and preserved in an airtight container.

In PLAL, The CdS target used were carried out on samples in the form of disc of about 0.85cm diameter and 0.16cm thick. It was positioned inside a cuvette (inner dimensions 10×10×35mm) (Suprasil 300 quartz) and held firmly in a holder place with a flexible thin teflon ring which was placed at the bottom of the cuvette, acting as a spring and pushing the sample onto its vertical wall. The cuvette was filled with de-ionized water. It was then placed onto a moving stage which could be moved in the x, y and z directions with accuracy of ±5μm. The Nd:YAG solid state laser was focused onto the target material surface using a lens of focal length 7cm by varying the energy of laser from 100mJ to 385mJ. Laser ablation was carried out by scanning the sample.The ablation was

carried out for15 minutes and formation of nanostructures in the solution could be confirmed by the slight change of the color of the solvent during ablation.

4. Results and Discussions

4.1. Transmission Electron Microscope

In CPM, In order to prove the key role of en in the formation of CdS nanostructures in aqueous solution, it is important to study the effect of varying the volume ratio of en with respect to distilled water (en: distilled water) used as a medium. Figures 1:3 show the TEM images of CdS nanostructures using 25%, 50%, and 100% of en dissolved in distilled water as a solvent. Figures1:2 show that CdS nanostructures tripods and nanorods are produced. While figure 3 and its histogram shows that the using of 100% en CdS nanostructures produced in spherical shape and particles size is 45nm. So, from these figures, it can be seen that as the volume ratio of en increases from 25% to 100% the growth of 1D (multirods) decreases in their axis to be 1D (nanorods) till they become spherical nanostructures at 100% en. It seems that en concentration strongly affects the length of the growing crystalline but much less acts on its diameter [28]. In en, the amine group (NH_2) is known to be a capping ligand that highly influences the morphology of nanoproducts through interactions with the metal centers on the surface of nanocrystals, thus changing the growth rates of different faces [29]. This capping ligand in en when interact with Cd cations, bidentate ligand complex $[Cd(en)_2]^{2+}$ is formed which served as a molecular template in control of the CdS crystal growth [30] and an intermediate in the control of the CdS crystal growth [31]. Moreover, lower concentration of en caused diffusion of more constituent elements inside the capping sphere, which was responsible for the particles size growth leading to increase in particle size of nanostructures [32]. Therefore at high concentration of en the complexes $[Cd(en)_2]^{2+}$ is very stable. So, the S ions were released slowly from the complex which gives much more time for forming the nanostructures. So, the nanostructures fabricated as spherical form due to it has the highest stable form. While with decreasing the concentration of en, the stability of the complexes $[Cd(en)_2]^{2+}$ decreased, the S ions were released rapidly and the growth in 1D form like uniform nanorods. While the further increasing of the concentration of en, the growth in 1D is appeared in the number of direction leading to formation of multirods [33].

Figure 4 shows TEM image of CdS nanostructures synthesized by ns laser (1064nm, 385mJ) ablation of CdS target immersed in deionized-water as a medium. The produced nanostructures are very small with the size in the range of 9.5nm with high homogeneity and narrow particle size distribution. This

happen because of the mechanism of laser matter interaction leading to laser induced material removal. This mechanism can basically be classified into two; thermal and non-thermal process. In thermal process, the type of pulsed laser is short laser pulses (Ns). The ablation process is dominant by heat conduction, melting, evaporation and plasma formation. This energy of the laser pulse is absorbed on the surface of the work piece and heat conduction leads to the formation of a temperature field. So, the nanostructures produced and appeared in nanosphereshape which represents the most stable form [34-38].

5. X-Ray Diffraction

Figure 5 shows the powder XRD patterns of CdS nanostructures precipitated from the aqueous solution at different amount of en dissolved in distilled water. From this figures it's clear that the more remarkable peaks were observed at 2θ = 25, 27, 29, 44, 48 and 52°. The discernible peaks can be indexed to (100), (002), (101), (110), (103), and (112) planes of the hexagonal structure of CdS according to the lattice constants close to the values in literature (JCPDS No. 01-0780) [39, 40]. A more precise examination and intercomparisons of diffraction patterns obtained for different nano CdS lead to three conclusions; First, the as-prepared samples are crystalline as seen by broad XRD features at prominent lattice planes of these materials rather than amorphous which would yield only a very broad single. Similar nonamorphous particles were made by Murray et al. [41]. Second, the XRD peaks of hexagonal CdS were broad in accordance with their small grain size and low degree of crystallinity. These nanocrystals have lesser lattice planes compared to bulk, which contributes to the broadening of the peaks in the diffraction pattern. This broadening of the peak could also arise due to the micro-straining of the crystal structure arising from defects like dislocation and twinning. These defects are believed to be associated with the chemically synthesized nanocrystals as they grow spontaneously during chemical reaction [42].Third, no characteristic peaks were observed for the other impurities, such as $CdCl_2$ or Na_2S which may reflect the purity extent of prepared CdS nanostructures. However, one can see weak shoulders corresponding to (100) (2θ = 25°) and (101) (2θ = 29°) peaks of wurtzite phase riding over the (002) peak of the hexagonal phase suggesting the presence of small fraction of wurtzite phase in the synthesized sample.

Figure 6 shows the powder XRD patterns of CdS nanostructures prepared by PLAL. From this figure it's clear that the more remarkable peaks were observed at 2θ = 24, 26, 28, 43 and 51°. The discernible peaks can be indexed to (100), (002), (101), (110), and (112) planes of the hexagonal structure of CdS according to the lattice constants close to the values in

literature (JCPDS No. 01-0780). Moreover, No characteristic peaks were observed for the other impurities, such as S or Cd which may reflect the purity extent of the prepared CdS nanostructures.

5.2. UV-VisibleAbsorption Spectra

The optical properties of materials are very sensitive to the transition from bulk materials to low-dimensional systems. The II–VI nanostructures are well known to exhibit a strong change of their optical absorbance when their size is reduced to a few nanometers [43]. Figure 7 shows the UV-Visible absorption spectrum of CdS nanostructures synthesized by CPM at a different percentage of en and 1:7 Cd:S molar ratio at 80°C. From this figure it's clear that as the percentage of en increased from 25% to 100%, the maximum wavelength (λ_{max}) increased from 435nm to 490nm.This figure exhibits a broad absorption peak in the spectral region which is assigned to the optical transition of the first excitonic state. This band is due to the first optically allowed transition of CdS between the electronic state in the conduction band (CB) and the hole state in the valence band (VB). And these values are different than that of the bulk CdS, which is usually observed around 515 nm due to the quantum size effect of CdS nanostructures [41]. This clearly depicts that size of the nanocrystals formed are governed by precipitation of Cd^{2+}cations with S^{2-} anions in aqueous solution in the presence of a stabilizer. The decrease in the particle size results in the increase in the band gap between the VB and CB. Consequently, the excitation of electron from VB to CB requires higher energy, which results in the blue shift or light absorbance in higher energy region, i.e. lower wavelength region. The blue-shift in the energy band gap indicates increase in effective band of the samples [44]. So, It's clear from this figure that the band position of this peak was blue shifted gradually as the percentage of en increased, indicating quantum size effect i.e. formation of smaller particles [41, 45]. So, by tuning this percentage it is indeed possible to vary the growth rate at a particular instant of time.

The electron excitation from valance band (VB) to conduction band (CB), can be used to determine the nature and value of the optical band gap. The optical band gap has been estimated from absorption coefficient data as a function of wavelength by using Tauc Relation [46, 47]:

$$\alpha h\upsilon = B\left(h\upsilon - E_{np}\right)^{n} \qquad (3)$$

where α is the absorption coefficient, hν is the photon energy, B is band tailing parameter, E_{np} the optical band gap of the nanoparticle, and n = 1/2 for direct band gap.

It is well known that CdS is a direct band gap NP; hence the direct band gap value is estimated from the absorption spectra by plotting $(\alpha h\nu)^2$ versus $(h\nu)$ and extrapolating the straight line to the energy axis of the graph to hν axis i.e. at α = 0. Figure 8 shows the typical plots of $(\alpha h\nu)^2$ vs $(h\nu)$ for the prepared CdS nanostructures at a different percentage of en. It's clear from this figure that the x-intercept of a line (the point at which the line crosses the x axis) represent the energy band gap in the different percentage of en. So, the amount of en increased in the medium from 25% to 100%, the energy band gap decreased from 4.95ev (25% en) to 3.95ev (50% en) to 2.59ev (100% en).

The size of nanostructures can be estimated by applying Brus effective mass model on the Effective mass approximation formula (EMA) which given as [9, 48];

$$E_{g\,(nano)} = E_{g\,(bulk)} + \frac{\hbar^2\pi^2}{2R^2}\frac{1}{\mu} - \frac{1.786e^2}{4\pi\varepsilon_\circ\varepsilon R} - \frac{0.124e^4}{\hbar^2\varepsilon^2}\mu$$

$$,\frac{1}{\mu} = \frac{1}{m_e^*} + \frac{1}{m_h^*} \qquad (4)$$

$$\Delta E_g = E_{g(nano)} - E_{g(bulk)} = \frac{\hbar^2\pi^2}{2R^2}\frac{1}{\mu} - \frac{1.786e^2}{\varepsilon R} - \frac{0.124e^4}{\hbar^2\varepsilon^2}\mu \qquad (5)$$

where $E_{g(nano)}$ is estimated from absorption coefficient data as shown above, $E_{g(bulk)}$ is bulk band gap (2.4eV for CdS), h is Planck's constant, R is the radius of nanoparticle, m_e^* the effective mass of the electron ($0.19m_e$ for CdS), m_h^* the effective mass of the hole ($0.8m_e$ for CdS), m_e is the free electron mass (kg), e is the electronic charge (C), ε is the dielectric constant of nanoparticle (5.7 for CdS), $\varepsilon_\circ$ is the dielectric constant of vacuum ($C^2J^{-1}M^{-1}$), μ is the effective mass of the system, $\hbar = 6.58211928\times10^{-16}eVs^{-1}$, and $m_e = 0.510998928MeVc^{-2}$[49].

The second and third terms are much smaller than the first term, therefore may be neglected and the expression reduced. So, the increase in band gap in nanostructures due to quantum confinement has the equation form [49].

$$\Delta E_g = E_{g\,(nano)} - E_{g\,(bulk)} \approx \frac{\hbar^2\pi^2}{2R^2}\frac{1}{\mu} \qquad (6)$$

This equation can be used to estimate size of the particle taking proper value of μ and increase in band gap obtained from blue shift in absorption edge.

For hexagonal CdS, μ=1.919x10^{-31}Kg [50]. Substituting all the values and rearranging we get;

$$R = \frac{1.5606}{\Delta E^{1/2}} \quad (7)$$

The calculated average particles sizes were tableted in tables 1. From these tables it's clear that by varying the amount of en dissolved in distilled water, the calculated average particle sizes are 4.03nm, 31.21nm, and 8.66nm for 25%, 50%, and 100% of en dissolved in distilled water, respectively. So, the band gap energies gradually decrease from 4.95eV (25% en dissolved in dist. water) to 2.41eV (100% en).

In PLAL, figure 9 shows the small blue-shift of the absorption onset of the laser-ablated particles in comparison to that of the bulk indicates the presence of quantum confinement. The calculated average particle sizes using the particles size estimation were tableted in tables 2. From this table it's clear that the absorption edge increases from 2.6 nm: 5.92 nm by decreasing energies of laser from 385mJ:100mJ (seen in table 2). So, the band gap energy gradually decrease from 2.78eV (385mJ) to 2.49eV (100mJ) and shifted to the lower side of the spectrum. These changes have been attributed to the crystallite size-dependent properties of the energy band gap.

Conclusion

In CPM, with increasing the amount of en from 25% to 100% the produced nanorods decrease in their axis till they become spherical nanostructures at 100% of en. The powder X-ray diffraction (XRD) patterns of the different CdS nanoparticles indicated that the precipitated CdS have the hexagonal crystal structure. The systematic blue shift in the absorption edge of the UV-Visible with changing the particles size is observed. This shift is due to the quantum size effect of CdS nanostructures.

In PLAL, The production system of PLAL is easy, simple and cheap, does not require costly vacuum chambers. The ns laser ablation of CdS target immersed in deionized-water produce nanoparticles in the size range of 5nm with high homogeneity and narrow particle size distribution. The TEM images indicated that CdS nanostructures have an external spherical shape. PLAL can be applied in all materials because of its ability to ablate almost all kinds of materials due to the ultra-high energy density and control over the growth process by manipulating the process parameters like Intensity, wavelength.

References

1. N.G. Semaltianos, S.L., W. Perrie, S. Romani, R.J. Potter, M. Sharp, P. French, G. Dearden, K.G.Watkins, *II–VI semiconductor nanoparticles synthesized by laser ablation.* Journal of Appl. Phys. A, 2009. **94**: p. 641-647.
2. Gaponenko, S.V., *Optical Properties of Semiconductor Nanocrystals.* Cambridge Univ. Press, Cambridge, 1998.
3. J. Lin, S.F.L., S. Mahmood, T. L. Tan, S. V. Springham, P. Lee, and R. S. Rawat, 33rd EPS Conference on Plasma Phys. Rome, 2006. **301**.
4. Sylvestre, J.-P., et al., *Femtosecond laser ablation of gold in water - target position.* Journal of Appl. Phys. A, 2005. **80**: p. 753–758.
5. Sanz, M., et al., *Ultrafast Laser Ablation and Deposition of Wide Band Gap Semiconductors.* The Journal of Physical Chemistry C, 2011. **115**(8): p. 3203-3211.
6. O'Regan, B.G., M. , *A low-cost, high-efficiency solar cell based on dye-sensitized colloidal TiO2 films.* Nature, 1991(353): p. 737-740.
7. Z. K. Tang, G.K.L.W., P. Yu, M. Kawasaki, A. Ohtomo, H. Koinuma, and Y. Segawa, *Room-temperature ultraviolet laser emission from self-assembled ZnO microcrystallite thin films.* Appl. Phys. Lett., 1998(72): p. 3270.
8. D. M. Bagnall, Y.F.C., Z. Zhu, T. Yao, S. Koyama, M. Y. Shen, and T. Goto, *Optically pumped lasing of ZnO at room temperature.* Appl. Phys. Lett., 1997. **70**: p. 2230.
9. Brus, L.E., *Electron–electron and electron-hole interactions in small semiconductor crystallites: The size dependence of the lowest excited electronic state.* J. Chem. Phys., 1984(80): p. 4403.
10. T. Donnelly, S.K., K. Carney, N. McEvoy, J. G. Lunney, *Pulsed laser deposition of nanoparticle films of Au.* Applied Surface Science, 2007. **254**.
11. S. Yang, Y.J., C. H. Kim, C. Hwang , J. Lee , S. Chae , S. Jung , M. Choi, *A flame metal combustion method for production of nanoparticles.* Powder Technology, 2010. **197**.
12. C. Wu, X.Q., J. Chen, H. Wang, F. Tan, S. Li, *A novel chemical route to prepare ZnO nanoparticles.* Materials Letters, 2006. **60**: p. 1828–1832.
13. H. Jia, J.Z., W. Song, J. An, B. Zhao, *Preparation of silver nanoparticles by photo-reduction for surface-enhanced Raman scattering.* Thin Solid Films, 2006. **496**: p. 281–287.
14. P. Y. Lim, R.S.L., P. L. She, C. F. Hung, H. C. Shih, *Synthesis of Ag nanospheres particles in ethylene glycol by electrochemical-assisted polyol process.* Chemical Physics Letters, 2006. **420**: p. 304–308.

15. Pradeep, M.J.R.a.T., *Solvothermal synthesis of silver nanoparticles from thiolates.* Journal of Colloid and Interface Science, 2003. **268**: p. 81–84.
16. M. S. Chargot, A.G., A. Smolira, J. Cytawa, L. Michalak *Massspectrometric investigations of the synthesis of silver nanoparticles via electrolysis.* Vacuum, 2008. **82**: p. 1088–1093.
17. Yang, H.H.a.X., *Synthesis of polysaccharide-stabilized gold and silver nanoparticles: a green method.* Carbohydrate Research, 2004. **339**: p. 2627–2631.
18. J. Gu, W.F., A. Shimojima, T. Okubo *Microwave-induced synthesis of highly dispersed gold nanoparticles within the pore channels of mesoporous silica.* Journal of Solid State Chemistry, 2008. **181**: p. 957–963.
19. Y.Liu, L.L., W.Chiu, *Size-Controlled Synthesis of Gold NPs from Bulk Gold Substrates by Sonoelectrochemical Methods.* J. Phys. Chem. B, 2004. **108**: p. 19237-19240.
20. H. Eerikainen, E.K., *Preparation of polymeric nanoparticles containing corticosteroid by a novel aerosol flow reactor method.* International Journal of Pharmaceutics, 2003. **263**: p. 69–83.
21. K. L. McGilvray, M.R.D., D. Wang, J. Scaiano *Facile photothermal synthesis of unprotected aqueous gold nanoparticles.* J. Amer. Chem., 2006. **128**: p. 15980.
22. M. Duocastella, J.M.F.-P., J. Dominguez, P. Serra, J. L. Morenza, *Printing biological solutions through laser-induced forward transfer.* Appl Phys A, 2008. **93**: p. 941–945.
23. Y. Itoh, M.A.a.K.O., *Direct preparation of nonagglomerated indium tin oxide nanoparticles using various spray pyrolysis methods.* J. Mater. Res., 2004. **19**: p. 1077-1086.
24. Song-Yi Yang, S.-G.K., *Characterization of silver and silver/nickel composite particles prepared by spray pyrolysis.* Powder Technol., 2004. **146**(3): p. 185–192.
25. N. S. Tabrizi, M.U., V. A. Vons, U. Lafont, A. Schmidt-Ott *Generation of nanoparticles by spark discharge.* J. Nanopart Res, 2009. **11**: p. 315–332.
26. Barcikowski, S., Devesa, Francisco, Moldenhauer, and Kirsten, *Impact and structure of literature on nanoparticle generation by laser ablation in liquids.* Journal of Nanoparticle Research, 2009. **11**(8): p. 1883-1893.
27. Allmen, M.v. and A. Blatter, *Laser-Beam Interactions with Materials (Springer, Berlin, 1995), 2nd ed.*
28. Qiu-Lin Nie, Z.-D.X., Qiu-Li Yuan, Guo-Hua Li *Chemical control synthesis of CdS nanorods with different diameter.* Materials Chemistry and Physics, 2003(82): p. 808–811.
29. Jing Chen, L.C., and Li-Ming Wu, *The Solventless Syntheses of Unique PbS Nanowires of X-Shaped Cross Sections and the Cooperative Effects of*

Ethylenediamine and a Second Salt. . Inorg. Chem., 2007. **46**: p. 8038-8043.

30. Ya-Dong Li, H.-W.L., Yi Ding, Yi-Tai Qian, Li Yang, and Gui-En Zhou *Nonaqueous Synthesis of CdS Nanorod Semiconductor.* Chem. Mater., 1998 **10**(9): p. 2301.

31. Li, X.W.a.Y., *Solution-Based Synthetic Strategies for 1-D Nanostructures.* Inorg. Chem., 2006(45): p. 7522-7534.

32. Soumitra Kar, C.P., and Swadeshmukul Santra, *Direct Room Temperature Synthesis of Valence State Engineered Ultra-Small Ceria Nanoparticles: Investigation on the Role of Ethylenediamine as a Capping Agent.* J. Phys. Chem. C, 2009. **113**(12): p. 4862–4867.

33. Yadong Li, H.L., Yi Ding, Yue Fan, Yue Zhang, and Yitai Qian, *Solvothermal Elemental Direct Reaction to CdE (E) S, Se, Te) Semiconductor Nanorod.* 1999. **38**: p. 1382-1387.

34. *Effect of aging on copper nanoparticles synthesized by pulsed laser ablation in water: structural and optical characterizations.* Mater. Sci., 2011. **34**(7): p. 1363–1369.

35. D. Devaux, R.F., L. Tollier, and E. Bartnicki, *Generation of shock waves by laser-induced plasma in confined geometry.* J Appl Phys 1993. **74**(4): p. 2268-2273.

36. P. Peyre, R.F., *Laser shock processing: a review of the physics and applications.* Optics Quantum Electron 1995. **27**(12): p. 1213-1229.

37. L. Berthe, R.F., P. Peyre, L. Tollier, and E. Bartnicki, *Shock waves from a water-confined laser-generated plasma.* J Appl Phys 1997. **82**(6): p. 2826-2832.

38. P Peyre, L.B., X Scherpereel, R Fabbro, *Laser-shock processing of aluminium-coated 55C1 steel in water-confinement regime, characterization and application to high-cycle fatigue behaviour.* J Mater Sci 1998. **33**(6): p. 1421-1429.

39. M. Chen, Y.X., J. Lu, Y. Xiong, S. Zhang, Y. Qian, X. Liu, J. Mater. Chem., 2002. **12**(748).

40. Wenlong Wang, a.F.B., *A Simple Aqueous-Solution Processing Route to Prepare Quantum-Confined CdS Nanorods.* CHEMPHYSCHEM, 2003(4): p. 761.

41. C. B. Murray, D.J.N., M. G. Bawendi, *Generation of shock waves by laser-induced plasma in confined geometry.* J. Am. Chem. Soc., 1993(115): p. 8706-.

42. H. C. Warad, S.C.G., B. Hemtanon, C. Thanachayanont, J. Dutta, *Luminescent nanoparticles of Mn doped ZnS passivated with sodium hexametaphosphate.* Sci. Tech. Advanc. Mater., 2005. **6**: p. 296.

43. C. Unni, D.P., K. G. Gopchandran, *Studies on optical absorption and photoluminescence of thioglycerol-stabilized CdS quantum dots* Spectrochim. Acta A, 2008. **71**(4): p. 1402-1407.

44. V. NOGRIYA, J.K.D., M. RAMRAKHIANI, B. P. CHANDRA, *ELECTRO- AND PHOTO-LUMINESCENCE STUDIES OF CdS NANOCRYSTALS PREPARED BY ORGENOMETALLIC PRECURSOR.* Chalcogenide Letters, 2008. **5**(12): p. 365 – 373.

45. Wenzhong Wang, I.G., and M. Samy El-Shall, *Room-Temperature Synthesis and Characterization of Nanocrystalline CdS, ZnS, and CdxZn1-xS.* Chem. Mater, 2002. **14**(7): p. 3028–3033.

46. J. O. Winter, N.G., S. Gatzert, C. E. Schmidt, B. A. Korgel,, *Variation of cadmium sulfide nanoparticle size and photoluminescence intensity with altered aqueous synthesis conditions.* Colloids and Surfaces A: Physicochem. Eng. Aspects, 2005. **254**(1-3): p. 147-157.

47. K. S. Babu, C.V., P. Haridoss, *The influence of parameters of chemical synthesis on the optical properties of CdS nanocrystals.* Mater. Res. Bull., 2007. **42**(7): p. 1251–1261.

48. Kousik Duttaa, S.M., S.K. Deb, *Optical and electrical characterizations of ZnS nanoparticles embedded in conducting polymer.* Synthetic Metals, 2009. **159**(3-4): p. 315–319.

49. Kayanuma, Y., *Quantum-size effects of interacting electrons and holes in semiconductor microcrystals with spherical shape.* Phys. Rev.B., 1988. **38**.

50. R.Jayakrishnan, R.B.a., *Effect of the size-induced structural transformation on the band gap in CdS nanoparticles.* J. Phys. Condens. Mater., 2000. **12**(50).

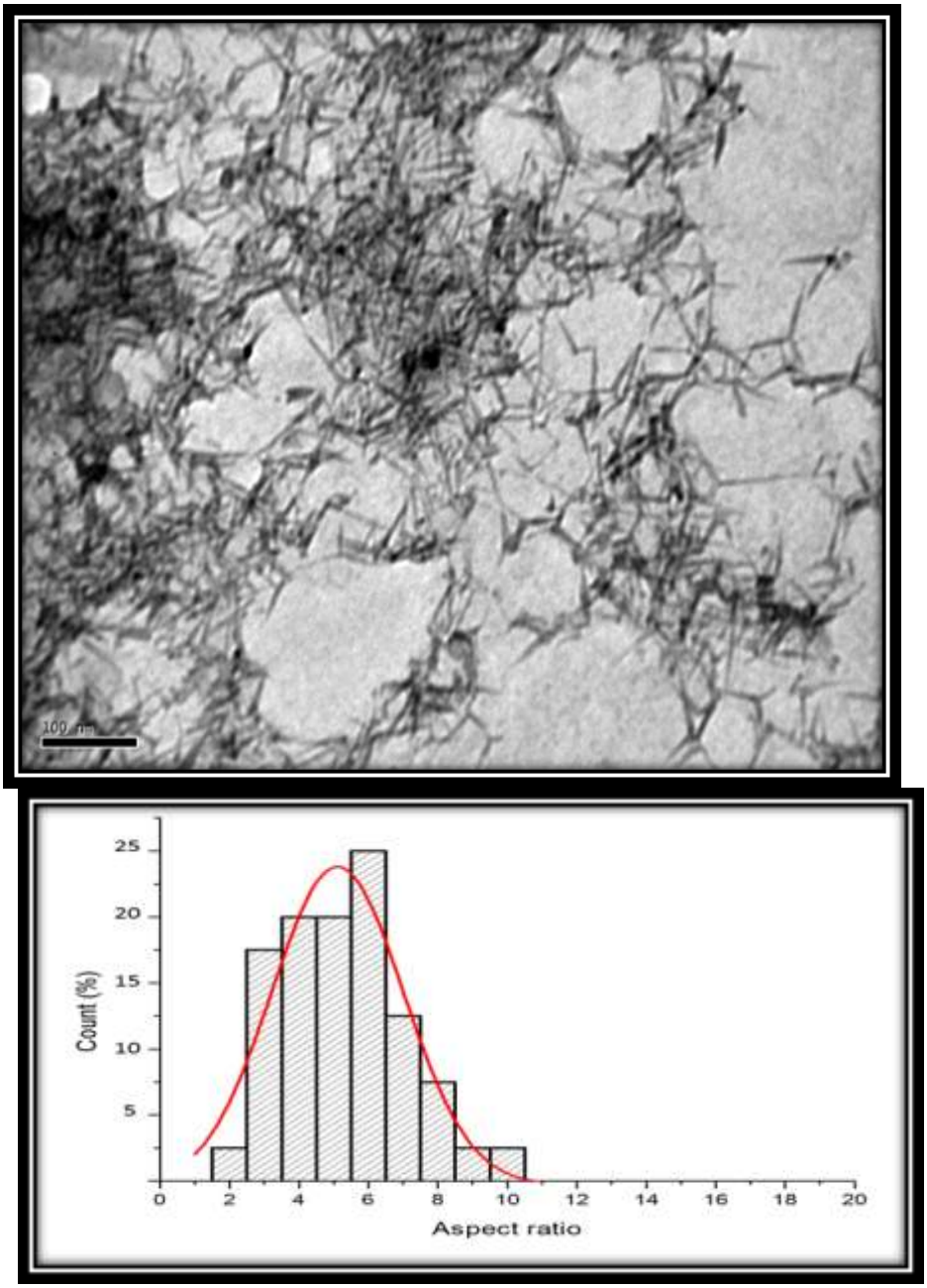

Figure 1: TEM image of CdS nanostructures prepared using Cd:S molar ratio of 1:7 at 80 °C for 24 hours dissolved in distilled-water containing 25% of en and its histogram of the aspect ratio

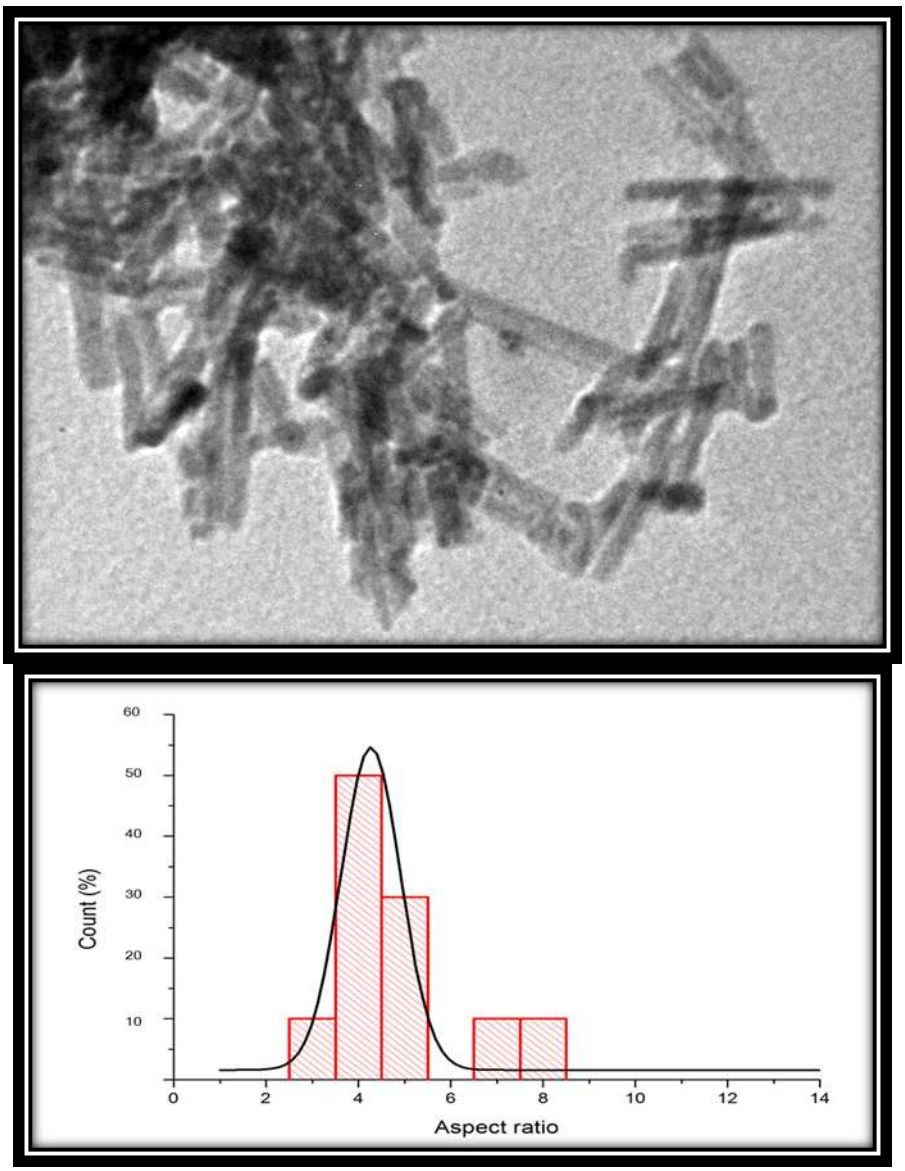

Figure 2: TEM image of CdS nanostructures prepared usingCd:S molar ratio of 1:7 at 80 °C for 24 hours dissolved in distilled-water containing 50% of en and its histogram of the aspect ratio

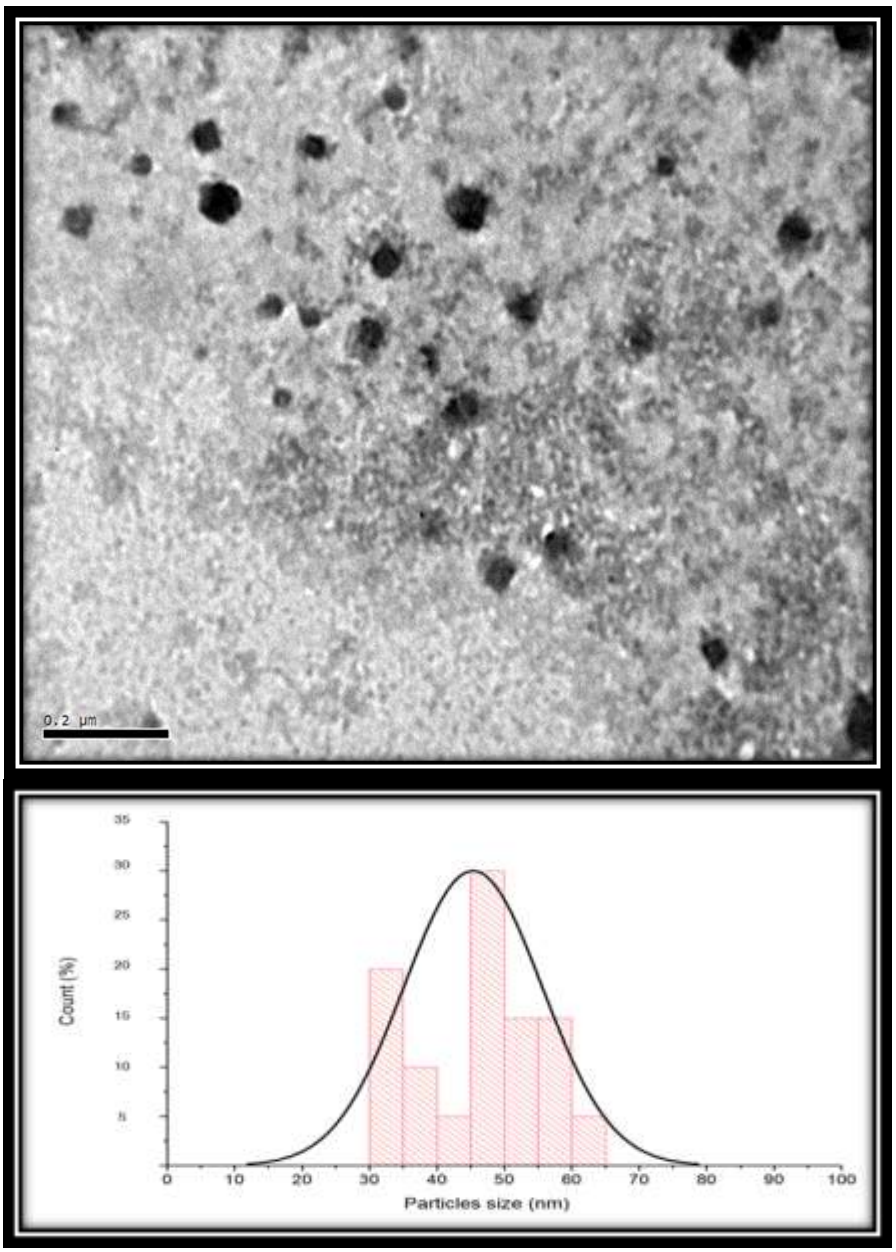

Figure 3: TEM image of CdS nanostructures prepared usingCd:S molar ratio of 1:7 at 80 °C for 24 hours dissolved in 100% of en and its histogram of the particles size

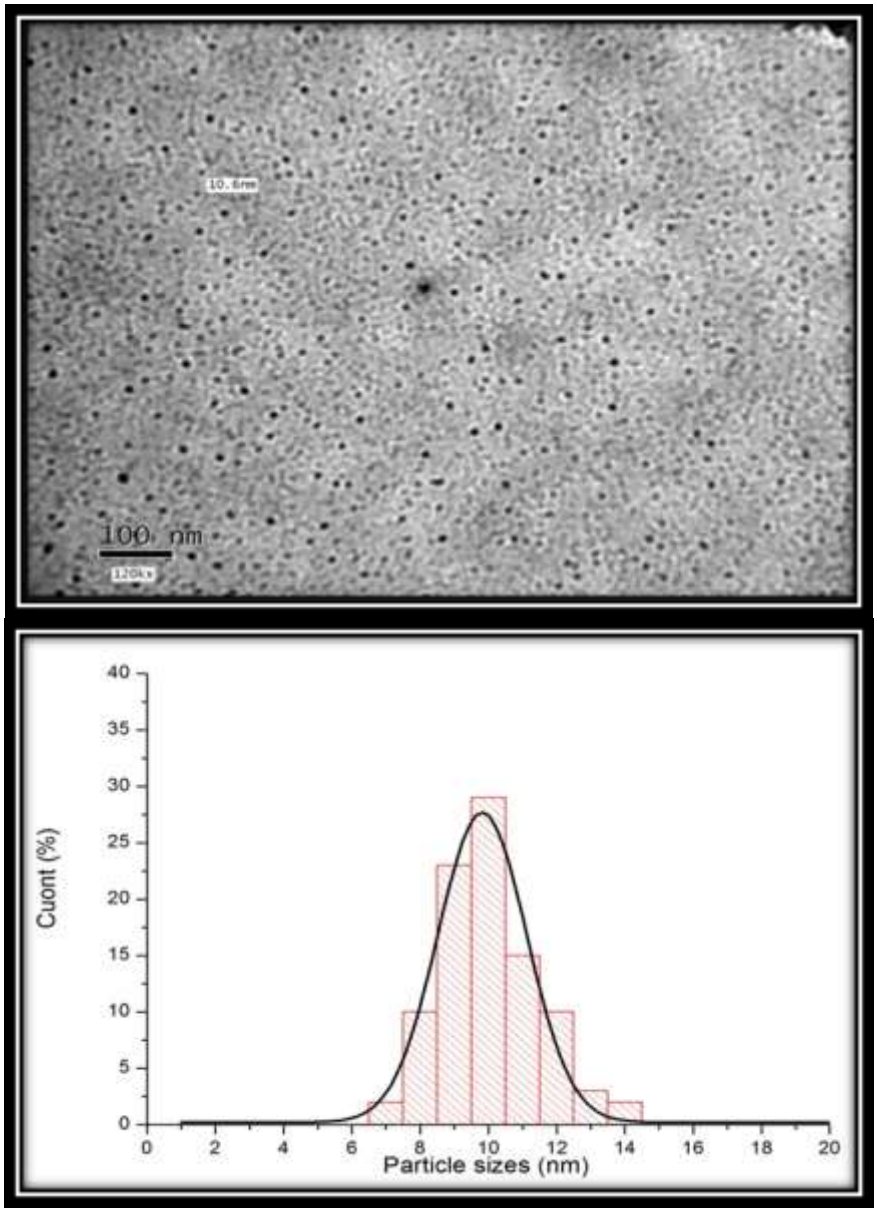

Figure 4: TEM image of CdS nanostructures produced by ns PLAL using CdS-tablet immersed in deionized solution and its histogram of particles size

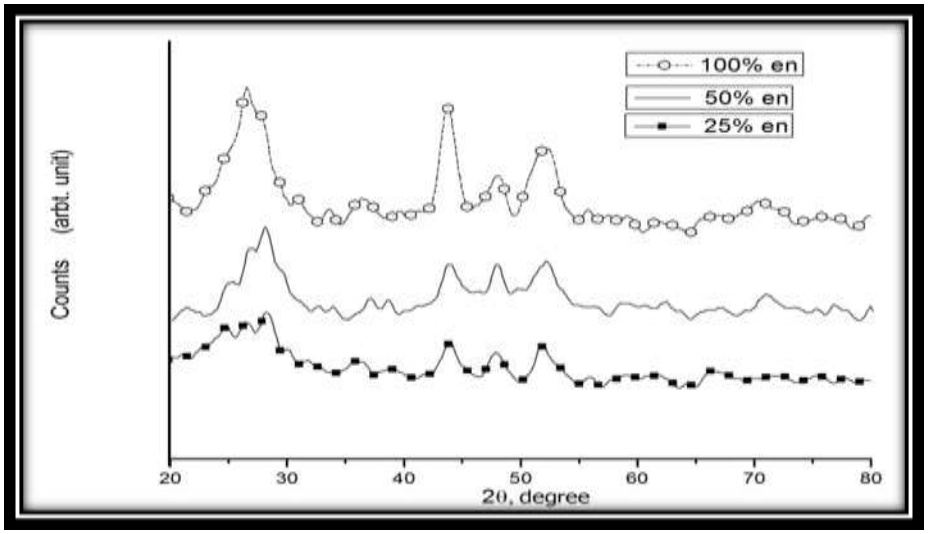

Figure 5: XRD pattern of CdS nanostructures prepared at Cd:S molar ratio of 1:7 and 80 °C for 24 hours at different amount of en dissolved in distilled-water

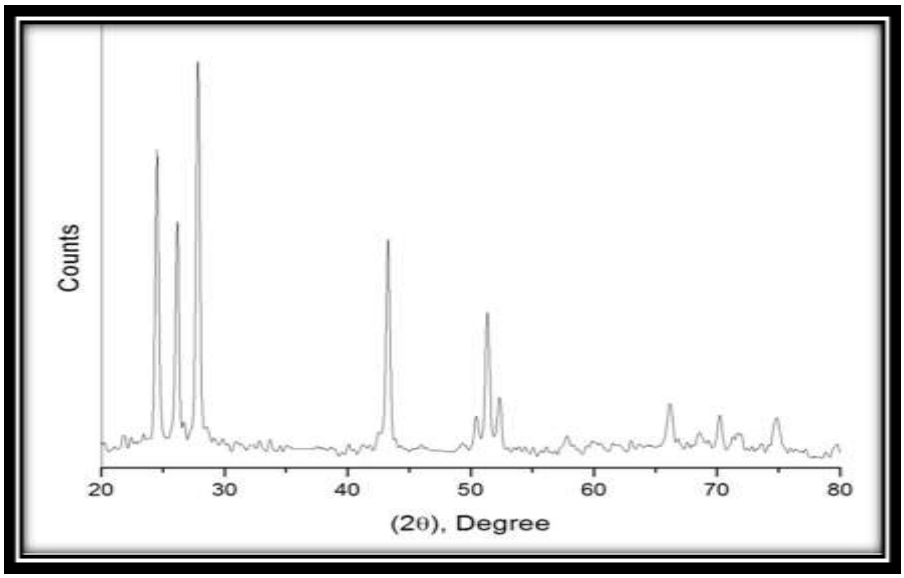

Figure 6: XRD pattern of CdS nanostructures prepared by PLAL

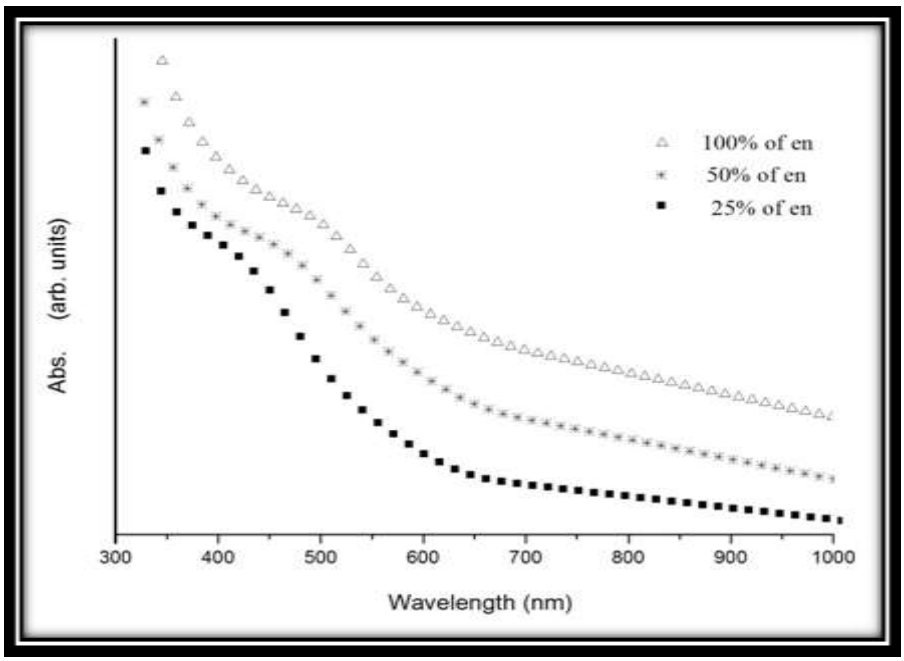

Figure 7: UV-Visible spectra of CdS nanostructures synthesized by chemical method at a 1:7 Cd:Smolar ratio dissolved in a different percentage of en (80 °C)

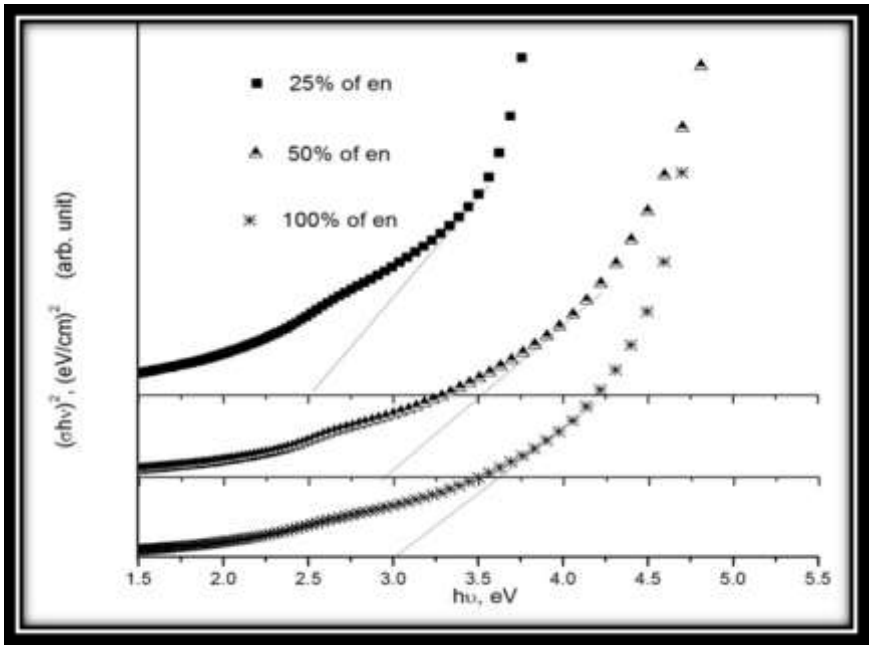

Figure 8: Typical relation of $(\alpha h\nu)^2$ vs $h\nu$ for CdS nanostructures prepared at different percentage of en

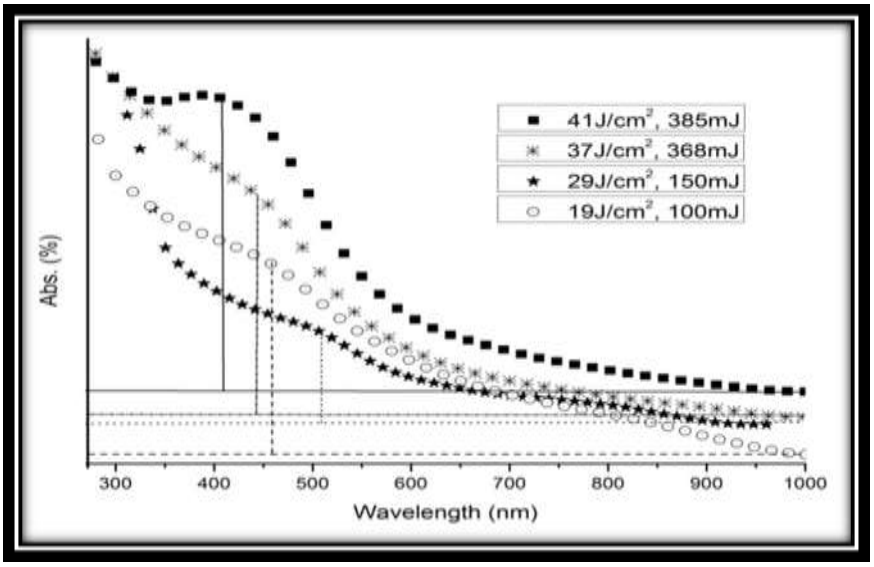

Figure 9: UV-Visible absorption spectrum of synthesized CdS nanostructures by Top-Down PLAL technique (ns-laser, 100mJ:385mJ)

Table 1: The optical parameters of CdS nanostructures produced by PLAL at different amount of en dissolved in dist. water.

Percentage of en (%)	**λ_{abs} (nm)**	**λ_{max} (nm)**	**E_{np} (eV)**	**R (nm)**	**D (nm)**
25	**572**	**429**	**4.95**	**2.01**	**4.03**
50	**590**	**463**	**3.95**	**2.10**	**4.21**
100	**604**	**503**	**2.41**	**15.6**	**31.21**

Table 2:The optical parameters of CdS nanostructures produced by PLAL (Top-Down technique)

Ns-laser	Energy of laser (mJ)	λ_{abs} (nm)	λ_{max} (nm)	E_{np} (eV)	R (nm)	D (nm)
w n te	385	595	409	2.78	2.61	5.2

	368	606	454	2.72	2.86	5.7
	150	666	477	2.64	3.34	6.7
	100	678	509	2.49	5.92	11.8